



# The impacts of Brewer-Dobson and Hadley circulation on tropospheric ozone variations over three city clusters in China



Xin Zhang <sup>a,b</sup>, Xingying Zhang <sup>b,\*</sup>, Lihua Zhou <sup>c</sup>, Xifeng Cao <sup>a,b,d</sup>, Zhili Deng <sup>a,b</sup>, Yuhang Jiang <sup>a,b</sup>

<sup>a</sup> China Academy of Meteorological Sciences, China Meteorological Administration, Beijing 100081, China

<sup>b</sup> Key Laboratory of Radiometric Calibration and Validation for Environmental Satellites, National Satellite Meteorological Center (National Center for Space Weather) and Innovation Center for FengYun Meteorological Satellite (FYVIC), China Meteorological Administration (CMA), Beijing 100081, China

<sup>c</sup> Department of Earth System Science, Tsinghua University, Beijing 100084, China

<sup>d</sup> Department of Atmospheric and Oceanic Sciences, Fudan University, Shanghai 200438, China

## ARTICLE INFO

### Keywords:

China  
Tropospheric column ozone  
Brewer-Dobson circulation  
Hadley circulation  
CCM

## ABSTRACT

The positive trend of tropospheric column ozone (TCO) in China has been confirmed by numerous observations, particularly in the rapidly developing city clusters such as Beijing-Tianjin-Hebei (BTH), the Yangtze River Delta (YRD) and the Pearl River Delta (PRD). An unignorable but poorly known function may be played by the Brewer-Dobson circulation (BDC) and the Hadley circulation (HC), both of which are in their strengthening phase. This study discusses their connection to TCO in these three city clusters based on a novel and powerful causal analysis method Convergent Cross Mapping (CCM). It revealed that both BDC and HC exerted substantial causal effects on the variations of the TCO in BTH, the YRD, and the PRD. The upwelling moving northward in the summer substantially lowered TCO in the PRD, contributing to the difference in the TCO annual cycle characteristics between northern and southern China. Besides, CCM distinguished that hemispheric HC impacts TCO greatly more than total HC, and the most essential branches of BDC were stratospheric or shallow branches. The BDC and HC indices determined by CCM were used for building a multiple linear regression model, which assessed their importance for long-term changes in regional TCO. The intensity of BDC is the most important influencing factor in each region, particularly in the YRD. BTH is mainly affected by the intensity of the two meridian circulations. The influence of the widths of meridional circulation upwellings on TCO in the PRD cannot be ignored. Furthermore, TCO displayed significant positive trends during 2005–2020, with rates of  $2.3 \pm 0.4$ ,  $2.5 \pm 0.4$ , and  $2.7 \pm 0.5$  DU/decade in BTH, the YRD, and the PRD, respectively.

## 1. Introduction

The increase in Tropospheric ozone ( $O_3$ ) has been widely observed by remote sensing and in-situ sites since 2000, particularly in East Asia. (Cooper et al., 2014). According to the Report on the State of the Ecology and Environment in China, the number of days with  $O_3$  as the primary pollutant has gradually caught up with and surpassed that of  $PM_{2.5}$  in recent years, especially in the rapidly developing city clusters, including Beijing-Tianjin-Hebei (BTH) and the Yangtze River Delta (YRD), and the Pearl River Delta (PRD) (MEEPRC, 2022). High concentrations of  $O_3$  in the low troposphere are harmful to humans, animals (Nuvolone et al., 2018), and even the whole natural ecosystems (Grulke and Heath, 2020). Furthermore, tropospheric  $O_3$  is one of the key greenhouse gases which comes in third place in terms of anthropogenic radiative forcing

(IPCC, 2021). Thus, the variation of tropospheric  $O_3$  and its influencing factors has drawn a great deal of attention.

The photochemical production within the troposphere and stratospheric downward dynamic transport through the stratosphere-troposphere exchange (STE) are recognized as two primary sources of tropospheric  $O_3$  (Banerjee et al., 2014; Danielsen, 1968; Stevenson et al., 2013). Although in situ photochemistry largely controls the abundance and distribution of tropospheric  $O_3$  (Lelieveld and Dentener, 2000), the role of STE should not be overlooked. STE drives 7–8 Dobson units (DU) in tropospheric  $O_3$  seasonal fluctuations in the Northern Hemisphere (Hsu and Prather, 2009). Based on a chemistry transport model, Hsu et al. (2005) diagnosed that the importance of STE for tropospheric  $O_3$  in East Asia is comparable to anthropogenic chemical production.

From a global and long-term perspective, atmospheric meridional

\* Corresponding author.

E-mail address: [zxy@cma.gov.cn](mailto:zxy@cma.gov.cn) (X. Zhang).

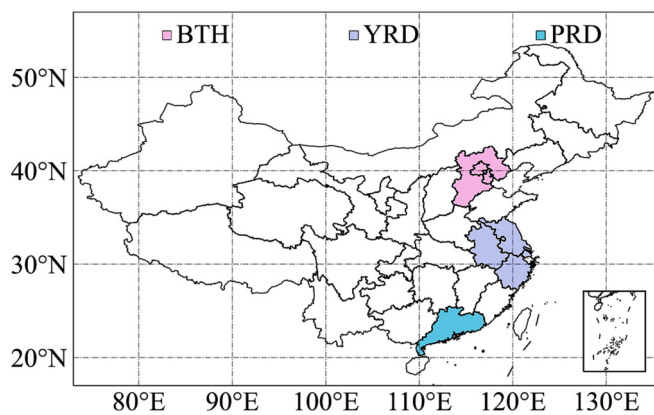


Fig. 1. Three major city clusters in China.

circulation is the key channel for STE (Holton et al., 1995; Stohl et al., 2003). An organized upwelling rises into the stratosphere in the tropics, and mass flux transported downward from the stratosphere to the troposphere occurs in middle and high latitudes. In the zonally averaged sense, this corresponds to the Brewer-Dobson circulation (BDC) (Stohl et al., 2003). In addition to transporting O<sub>3</sub> vertically, BDC acts on photochemical reactions indirectly by affecting air temperature during adiabatic exercise (Charlesworth et al., 2019) and changing atmospheric oxidation (Stohl et al., 2003). Satellite observations confirm that BDC is crucial in regulating seasonal variations in tropospheric O<sub>3</sub> in East Asia (Liu et al., 2015). It has been demonstrated that BDC is accelerating due to climate change and the growing chemical depletion of stratospheric O<sub>3</sub> (Butchart, 2014; Fu et al., 2015; Lin and Fu, 2013), which makes its impact on TCO in mid-latitude and high-latitude countries even more noteworthy. As the meridional circulation in the troposphere, Hadley circulation (HC) covers roughly half the surface area of the planet, which has helped shape the history of humanity by regulating precipitation (Webster, 2004). Both observations and simulations have demonstrated that the HC has experienced a poleward expansion in both hemispheres (Hu and Fu, 2007; Hu et al., 2013), which can explain more than half of the tropospheric O<sub>3</sub> trends observed in the extratropical southern hemisphere (Lu et al., 2019b). However, due to the significant interference from anthropogenic emissions, the impact of HC on tropospheric O<sub>3</sub> has seldom been studied in the northern hemisphere.

Compared to ground-based observations and O<sub>3</sub> sounding, satellite remote sensing has significant advantages in TCO research because of its excellent spatial and temporal coverage and continuity. The residual method, which defines TCO as the difference between total O<sub>3</sub> column (TOC) and stratospheric column O<sub>3</sub> (SCO), is the most commonly used TCO inversion algorithm in extratropical regions. The Total O<sub>3</sub> Mapping Spectrometer/Stratospheric Aerosol and Gas Experiment (TOMS/SAGE) provided the earliest combination of TOC and SCO (Fishman and Larsen, 1987). Since then, various combinations including TOMS/Halogen Occultation Experiment (HALOE), Solar Backscattered Ultraviolet (SBUV)/SAGE, SCanningImaging Absorption spectroMeter for Atmospheric CHartographY (SCIAMACHY)-nadir/limb, the Ozone Monitoring Instrument/Microwave Limb Sounder (OMI/MLS), Infrared Atmospheric Sounding Interferometer/Fast Optimal Retrievals on Layers for IASI (IASI/FORLI) have gradually been utilized to retrieve TCO (Ebojie et al., 2016; Fishman et al., 2003; Wespes et al., 2016; Ziemke et al., 1998; Ziemke et al., 2006). Hu et al. (2020) compared the TCO derived from various O<sub>3</sub> payload measurements using different inversion techniques and indicated that the residual technique combined with OMI/MLS is the best TCO algorithm for China. Therefore, it is also the most commonly used satellite data in current studies on TCO in China (Huang et al., 2013; Zhang et al., 2021).

To better understand the connection between TCO variations and BDC as well as HC in China, this study first analyzes the annual cycle

characteristics of TCO measurement from the OMI/MLS (2005–2020). Then, the causal influences of both the intensity and the upwelling width of the BDC and HC on TCO were examined based on Convergent Cross Mapping (CCM) and correlation analysis. Finally, a multiple linear regression (MLR) model was built to evaluate the roles of BDC and HC in constraining the TCO long-term variations.

## 2. Materials and methods

### 2.1. Study area

Numerous studies have proven the rising tropospheric O<sub>3</sub> in China, particularly in highly industrialized regions like Beijing-Shanghai-Guangzhou-Shenzhen, where extreme pollution events occur more frequently (Dufour et al., 2018; Fu et al., 2019; Huang et al., 2013). To reveal variations of TCO in highly industrialized regions in China and to further investigate the role of BDC and HC, this study focuses on three rapidly developing city clusters with severe O<sub>3</sub> pollution: BTH, the YRD, and the PRD (Fig. 1).

### 2.2. Data sources

In this study, monthly-mean gridded TCO product from January 2005 to December 2020, with a horizontal resolution of 1° × 1.25° (latitude × longitude), derived from OMI/MLS (Ziemke et al., 2006) was applied. Both OMI and MLS are aboard Aura satellite, avoiding accuracy errors caused by calibration between sensors of different satellite platforms. The row anomaly question of OMI has been corrected, and the 1σ precision for the TCO product was estimated to be about 1.3 DU (Ziemke et al., 2019).

Meridional wind ( $v$ ) data at 37 vertical layers (1000 hPa–1 hPa) was obtained from the ERA5 monthly averaged data on pressure levels dataset of the European Centre for Medium-Range Weather Forecasts (ECMWF) with a horizontal resolution of 0.25° × 0.25° (<https://cds.climate.copernicus.eu>) to measure BDC and HC. Tropopause pressure and vertical velocity ( $\omega$ ) from the National Centers for Environmental Prediction (NCEP) reanalysis dataset (<https://psl.noaa.gov/data/gridded/data.ncep.reanalysis.html>) with a resolution of 2.5° × 2.5° were utilized to calculate the vertical velocity at the tropopause by interpolation.

### 2.3. Data pre-processing

#### 2.3.1. BDC intensity and width indices

The Lagrangian-mean meridional mass transport by the BDC can be approximated by the transformed Eulerian mean stream function (Andrews and McIntyre, 1978), which defines residual meridional wind ( $\bar{v}^*$ ) in the pressure ( $p$ ) coordinate system as

$$\bar{v}^* = \bar{v} - \frac{\partial}{\partial p} \left( \frac{\bar{v}' \bar{\theta}'}{\bar{\theta}_p} \right) \quad (1)$$

where  $\bar{v}$  is the latitudinal mean of  $v$ ,  $\theta$  is the potential temperature,  $\bar{\theta}$  and  $\bar{\theta}'$  represent the latitudinal mean and eddy of  $\theta$ , respectively, and  $\bar{\theta}_p$  is the partial derivative of  $\bar{\theta}$  with respect to  $p$ . The intensity of BDC in the northern hemisphere can be measured by (Holton, 1990; Weiguo et al., 2015)  $F_{BDC}$ :

$$F_{BDC} = \frac{2\pi a \cos \varphi}{g} \int_0^p \bar{v}^* dp' \quad (2)$$

where  $a$ ,  $\varphi$ , and  $g$  represent the earth's radius, latitude, and gravitational acceleration, respectively. To determine the most influential BDC branch on TCO, we set three boundaries as the upper-limit pressure levels (100 hPa, 70 hPa, and 30 hPa) and obtain five BDC intensity (BDCI) indices corresponding to different BDC branches. They are BDC-

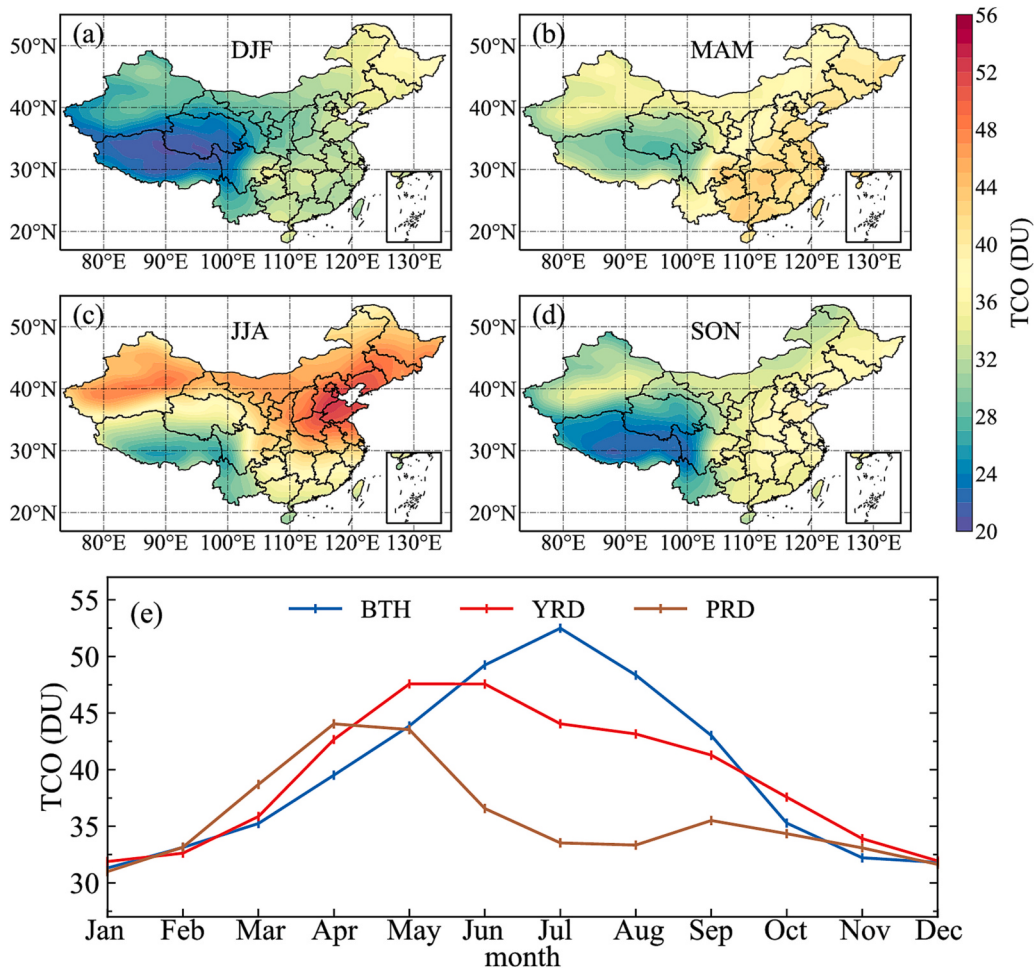


**Fig. 2.** (a-d) Seasonal variation of TCO across China and (e) annual cycle of TCO in BTH, the YRD, and the PRD.

total (100 hPa-), BDC-transition (100 hPa–70 hPa), BDC-stratospheric (70 hPa-), BDC-shallow (70 hPa–30 hPa), and BDC-deep (30 hPa-), respectively. More detailed definitions of various BDC branches can be found in (Lin and Fu, 2013). Regional BDCI in this study was spatially averaged according to located latitude ranges of study areas. At the latitudes where  $|F_{BDC}|$  maximum is located, the residual vertical velocity happens to turn around. Thus, the BDC turnaround latitudes in the northern and southern hemispheres (Hereinafter referred to as BDC-NTL and BDC-STL) correspond to the northern and southern boundary of its upwelling (Rosenlof, 1995). The width of BDC upwelling (BDCW) was defined as the difference between BDC-NTL and BDC-STL. Discussions about BDC upwelling boundaries and widths focus on the height of 70 hPa.

### 2.3.2. HC intensity and width indices

Similar to BDC, the mass flux stream function ( $F_{HC}$ ) can measure the intensity of HC intensity as.

$$F_{HC} = \frac{2\pi a \cos \varphi}{g} \int_0^p \bar{v} dp' \quad (3)$$

where physical variables correspond to the expression (2). NHC-500 and SHC-500 were defined as the maximum and minimum values of  $F_{HC}$  between  $40^\circ S$  and  $40^\circ N$  at 500 hPa, respectively, and THC-500 was derived by subtracting SHC-500 from NHC-500 (Pikovnik et al., 2022). Using these three HC intensity indices (HCI), this study compares the effects of northern and southern hemispherical HC (NHC and SHC) as well as total HC (THC) at the middle troposphere on TCO. In addition, the intensity of the NHC in the lower (925 hPa) and upper (250 hPa)

troposphere (NHC-925 and NHC-250) were taken into account to discuss the differences in impacts of HC at different altitudes on TCO. Similar to BDCW, HC width at 500 hPa (HCW) was defined as the difference between northern and southern turnaround latitudes (HC-NTL and HC-STL) at where the maximum values of  $|F_{HC}|$  were found.

## 2.4. Methods

### 2.4.1. Convergent Cross Mapping (CCM)

Convergent Cross Mapping (CCM) developed by Sugihara et al. (2012) diagnose the bidirectional causal coupling between two variables without interference from other processes in complex systems. The traditional Granger causality test identifies whether X causes Y by estimating the ability of “X to predict Y” (Granger, 1969), while the CCM method does the opposite. Sugihara et al. (2012) claim that in a nonlinear dynamic system, the responding process must contain all the information about the forcing process, however, the triggering process may not be the only predictor of the response process. Therefore, the correlation coefficient  $\rho$  between X predicted by the historical information of response variable Y and observed trigger variable X will increase with the increase of the time-series length L. The key to CCM diagnosis of causality lies in the convergence of predictive skill, that is, the correlation coefficient  $\rho$  increases with L and tends to stabilize after reaching the maximum. The correlation coefficient  $\rho$  is therefore used to quantify the strength of the causality. The prediction process in CCM is based on Takens’s theory (Takens, 2006) and state space reconstruction technology. Detailed principles and algorithms of CCM can be found in the study of Sugihara et al. (2012) and their introduction videos

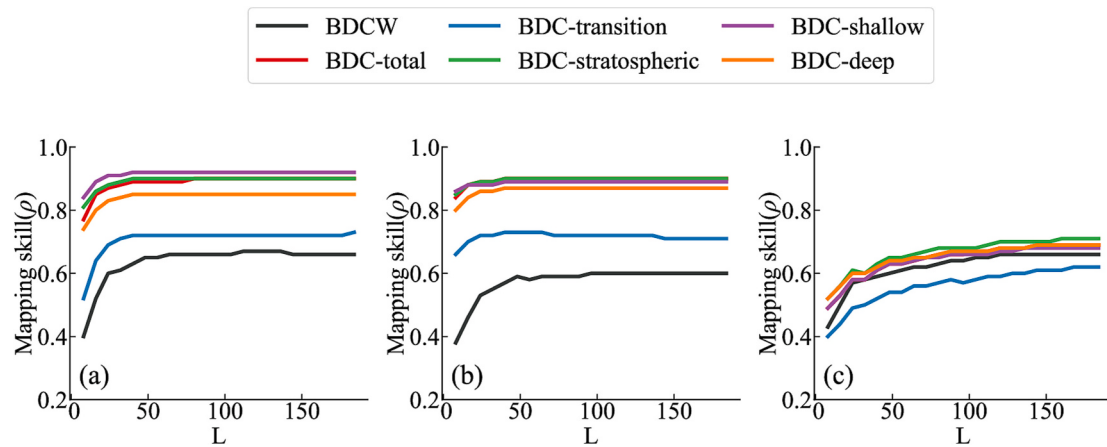


**Fig. 3.** Results of the TCO mapping BDC indices in (a) BTH, (b) the YRD, and (c) the PRD.

(<https://www.youtube.com/@sugiharalab>).

The method has been popular in quantitating causal links between various atmospheric system components since it is concise and powerful (Chen et al., 2019; Li et al., 2021), requiring only time series of the two variables. CCM has provided a more scientific research method for identifying the interaction effects of the climate system from the perspective of information flow and is anticipated to promote the transformation of model-driven causal inference technology into data-driven causal inference technology (Huajun and Guangjie, 2018).

This study concerns the unidirectional influence of meridian circulations on TCO; therefore, only the curve of the TCO mapping MCI, which stands for the causal influence of the meridian circulation index (MCI) on TCO was extracted. If the mapping curve is above the 0 line and converges as the observation library size increase, MCI will be judged to cause the change in TCO and the mapping skill of TCO mapping MCI ( $\rho_{MCI}$ ) will be used to indicate the intensity of the causal influence of MCI on TCO. Larger  $\rho_{MCI}/\rho_{MCI}$  represents a more substantial causal influence of MCI on TCO. The final BDCI and HCI, used for subsequent analyses, will be determined by the maximum values of  $\rho_{BDCI}$  and  $\rho_{HCI}$ . Additionally, the convergence rate also indicates the intensity of causality with the faster the curve converges, corresponding to the more vigorous the forcing effect.

#### 2.4.2. Multiple linear regression model (MLR)

Based on the indices that best reflect the causal influence of the meridian circulation on TCO determined by CCM analysis, an MLR model is established to quantify the role of BDC and HC on the long-term variation of TCO (Dufour et al., 2018; Zhou et al., 2019), which is expressed as

$$TCO_t = \alpha + \alpha_0 t + MCI_t + \varepsilon_t \quad (4)$$

where  $TCO_t$  is monthly mean TCO time series,  $t$  is the month sequence number (1–192),  $\alpha$  is the intercept,  $\alpha_0$  is the slope or linear trend, and  $\varepsilon_t$  is the error term.  $MCI_t$  represents time series of MCI terms selected by CCM, which is expressed as

$$MCI_t = \alpha_1 BDCI_t + \alpha_2 BDCW_t + \alpha_3 HCI_t + \alpha_4 HCW_t \quad (5)$$

where  $\alpha_{1-4}$  are the corresponding fit standardized coefficients. To mitigate the problem of multicollinearity in linear regression, the coefficients were estimated by ridge regression (Hilt and Seegrist, 1977). Adjusted R-square ( $R^2_{adjusted}$ ) was used to evaluate the goodness-of-fit indicated by the fraction of explained variation of MLR (Akossou, 2013):

$$R^2_{adjusted} = 1 - \frac{(1 - R^2)(n - 1)}{n - m - 1} \quad (6)$$

where  $n$  is the number of samples,  $m$  is the number of parameters,

and  $R^2$  is the coefficient of determination. The relative importance of each explanatory variable  $x_j$  is quantified based on its standardized regression coefficient in the expression:

$$x_j = \frac{|\alpha_j|}{\sqrt{\sum_{j=0}^4 \alpha_j^2}} \quad (7)$$

## 3. Results and discussions

### 3.1. Seasonal variation and annual cycle of TCO

The spatial distribution of seasonal mean TCO is depicted in Fig. 2 (DJF: December-the following February; MAM: March–May; JJA: June–August; SON: September–November). The compression of the tropospheric column atmosphere by the uplifting terrain is the fundamental reason for the considerable reduction of TCO in the Tibetan Plateau (Bian et al., 2011). High levels of TCO in northern China are primarily attributed to photochemical reactions related to anthropogenic and natural sources of emitted precursors (Tang et al., 2012; Wang et al., 2013). Similar to other parts of the northern hemisphere, TCO is significantly higher in the spring-summer than in autumn-winter, (Ebojie et al., 2016). Moreover, as the latitude moves from north to south, the season when the TCO peak appears shows a transition from summer to spring (Fig. 2b and Fig. 2c). The strong downward intrusions from the stratosphere at high latitudes in spring (Hsu and Prather, 2009; Ma et al., 2005) and the Asian summer monsoon (Wang et al., 2021; Zhao et al., 2010) are important dynamical attributions for this spatio-temporal distribution patterns of TCO.

The transition of the TCO peak season is more clearly shown in Fig. 2e, along with a shift of annual cycle switch from unimodal to bimodal from north to south. Besides, TCO levels and their amplitudes dropped from north to south, which is consistent with the observations of mountain sites that O<sub>3</sub> increased with the elevation of latitude in the northern hemisphere (Okamoto and Tanimoto, 2016; Wang et al., 2021). Global Atmosphere Watch stations also observed this latitude-dependent transition characteristic (Liu et al., 2019). The monthly mean TCO in BTH (denoted by TCO-BTH, and the meaning of position annotations is the same in the text below) displays a single peak in July of 52.5 DU. Photochemical processes in the low troposphere are considered the dominant factor for the summer peak in northern China (Fu et al., 2012; Yan et al., 2021). Transport from Northwest China also plays an important role (Gao et al., 2020). The TCO-PRD time series displays an evident bimodal characteristic, although the TCO-PRD in September (35.5 DU) is much smaller than in April (44.1 DU). High TCO-PRD levels in early spring are largely due to biomass burning (Liao

**Table 1**

The  $\rho\rho$  values of BDC indices on TCO in study areas diagnosed by CCM. The maximal  $\rho$  of BDCI indices are thickened, and the corresponding indices will be selected as the BDCI proxy.

	BTH	YRD	PRD
BDCW	0.66	0.60	0.66
BDC-total	0.90	0.90	0.70
BDC-transition	0.73	0.71	0.62
BDC-stratospheric	0.90	<b>0.91</b>	<b>0.71</b>
BDC-shallow	<b>0.92</b>	0.89	0.68
BDC-deep	0.85	0.87	0.69

et al., 2021). Besides, the East Asian monsoon contributes greatly to its summer trough (Wang et al., 2021). Despite the absence of a second peak, the high of the TCO-YRD lasts for two months (May–June), with the decline in August–September being considerably slowed down.

Summertime surface O<sub>3</sub> is sensitive to the predominant synoptic patterns in the YRD (Shu et al., 2020).

### 3.2. Causal impacts of meridian circulations on TCO in China

Several studies have reported the important impact of STE on tropospheric O<sub>3</sub> in northern and southern China, especially in the North China Plain (Ding and Wang, 2006; Lu et al., 2019a; Wang et al., 2020; Zhao et al., 2021). However, there are few studies on the contributions of BDC and HC, key channels of STE, to the TCO variations. Benefiting from CCM, a novel and powerful causal analysis method, this study attempts to explore their causal impacts on typical contaminated areas in China.

#### 3.2.1. The causal influence of BDC on TCO in China

Fig. 3 shows the results of the TCO mapping BDC indices diagnosed

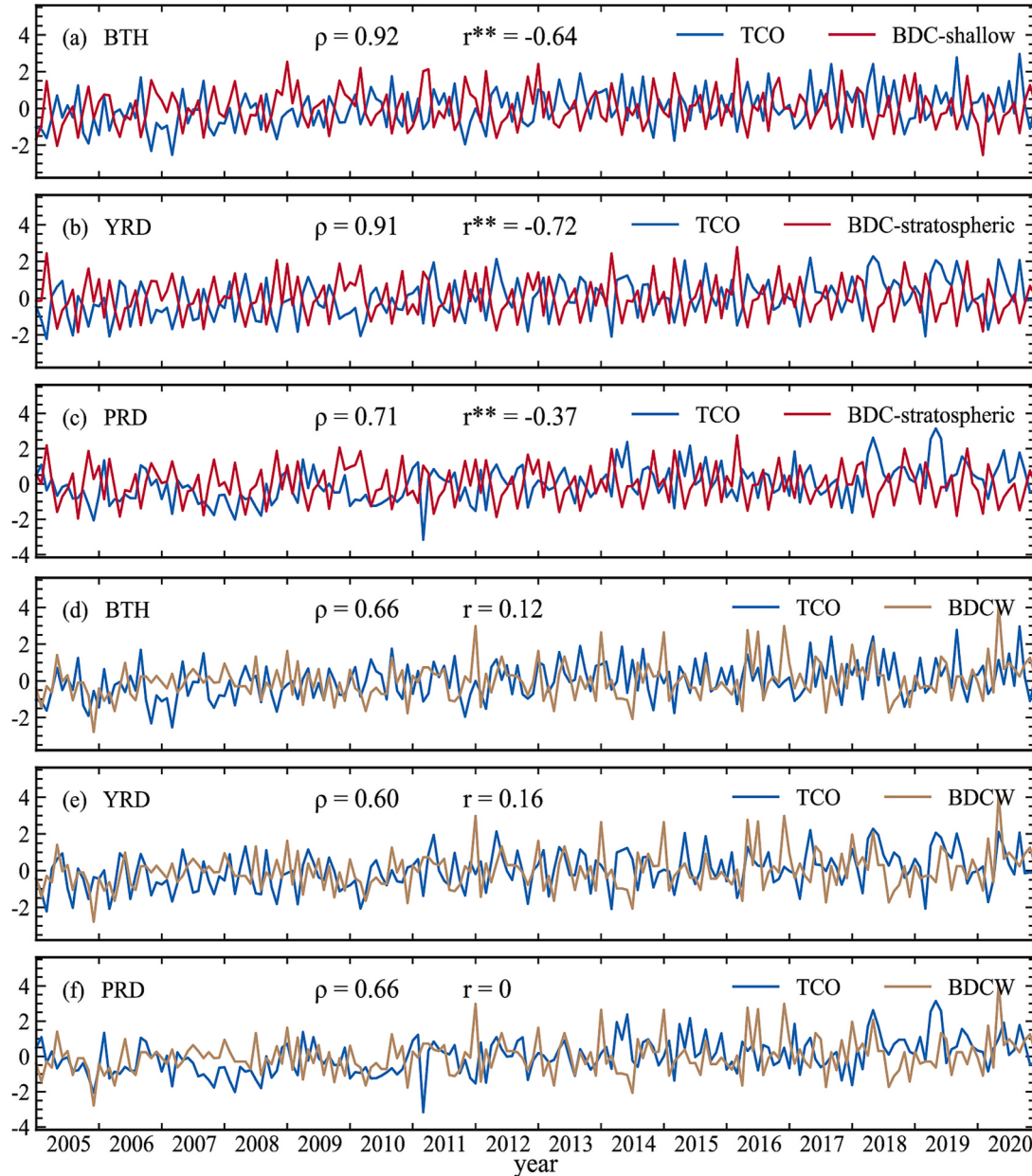


**Fig. 4.** Correlation between TCO and BDC indices with their standardized time series from 2005 to 2020. All of the time series have been deseasonalized and detrended. The  $\rho$  and  $r$  represent the strength of causality and linear correlation between the two variables, respectively. The ‘\*\*’ and ‘\*’ represent the correlation coefficient is statistically significant at the 99% and 95% confidence levels, respectively (similarly hereinafter).

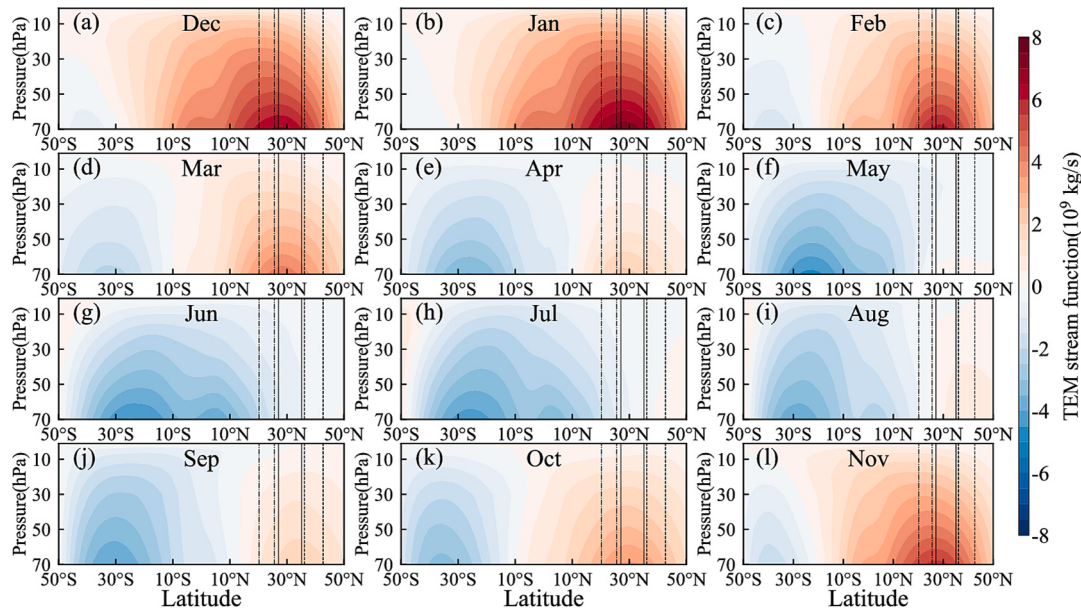


**Fig. 5.** The distribution of long-term monthly mean TEM stream function with latitude and altitude from 2005 to 2020, positive values represent the direction of the streamline is clockwise, and vice versa is counterclockwise. The latitude ranges covered by black dotted lines, solid lines, and dashed lines correspond to the location of BTB, the YRD, and the PRD, respectively.

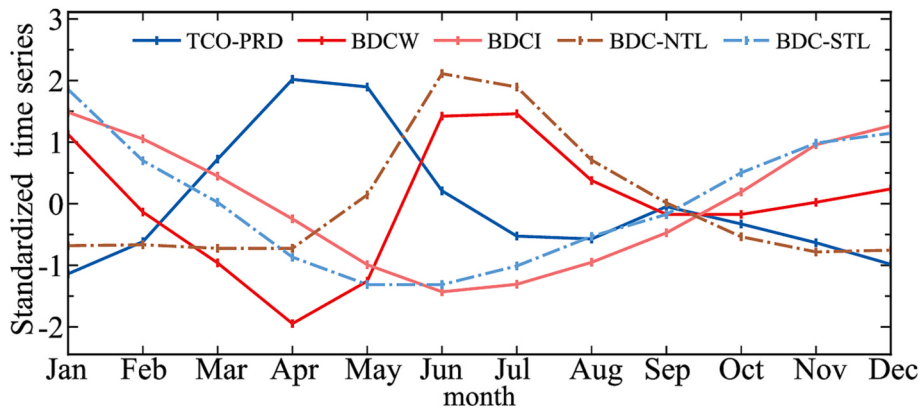


**Fig. 6.** Annual cycles of the TCO-PRD, BDCW, and BDC-NTL, BDC-STL.

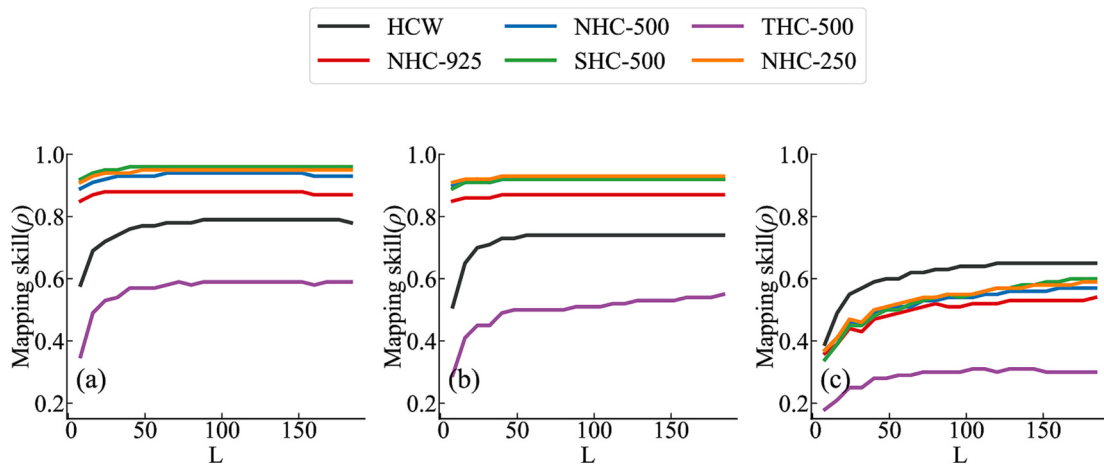


**Fig. 7.** The same as Fig. 3, but for HC.

**Table 2**

The same as Table 1, but for HC.

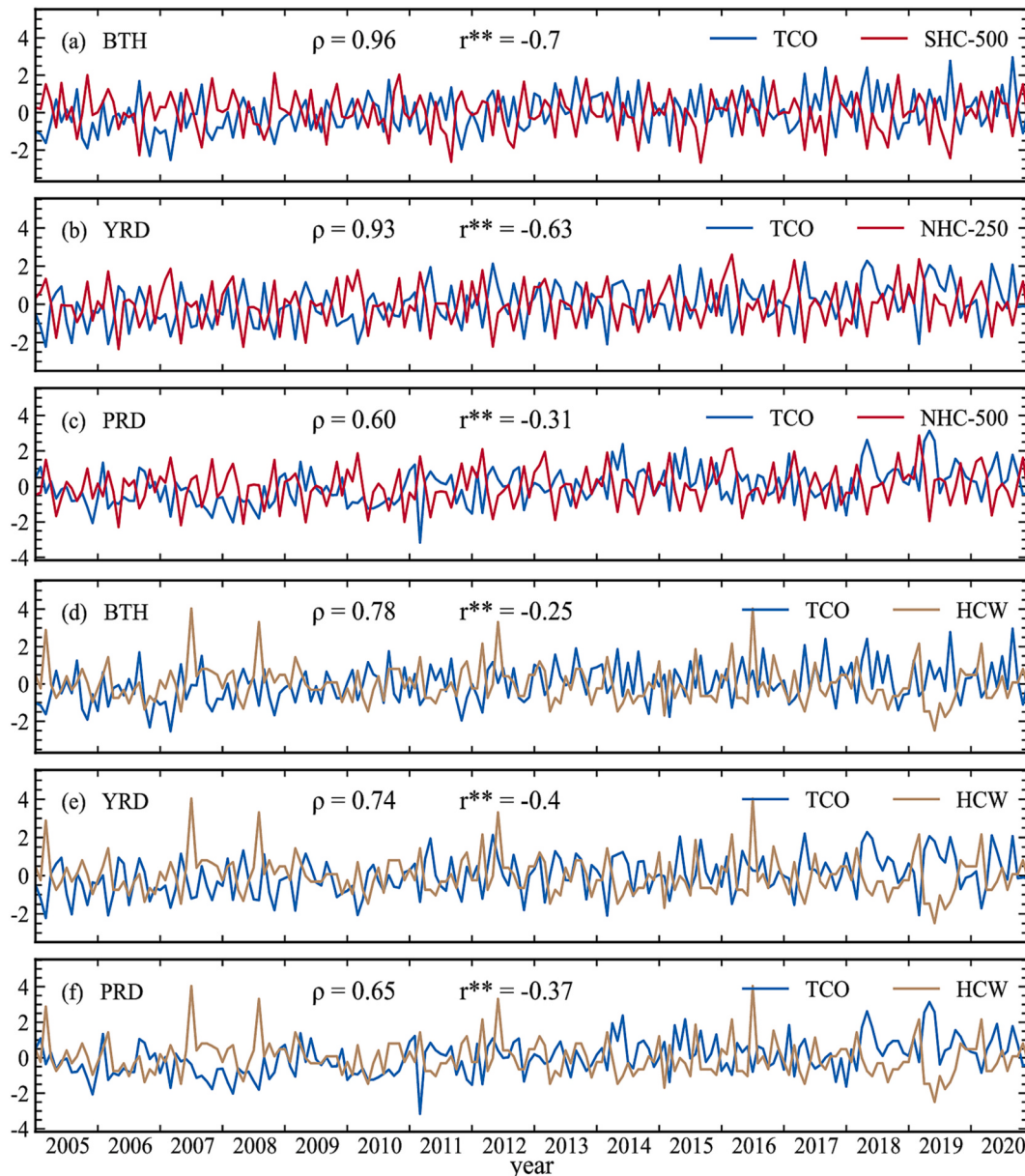
	BTH	YRD	PRD
HCW	0.78	0.75	0.65
NHC-925	0.87	0.87	0.54
NHC -500	0.93	0.92	0.57
SHC-500	<b>0.96</b>	0.92	<b>0.60</b>
THC-500	0.59	0.55	0.30
NHC -250	0.95	<b>0.93</b>	0.60

by CCM, and the causal influence strengths ( $\rho$ ) of all BDC indices are listed in Table 1. Stable convergence and high levels of  $\rho$  suggest that both the BDCI and BDCW drive TCO strongly. Among all the five branches, the impact of the transition branch is weakest whereas the other four have causal influence with roughly equivalent strengths on TCO. The BDC-shallow was chosen as the final proxy of BDCI in BTH for the shallow branch has the strongest causal influence (i.e., highest  $\rho$ ) on the local TCO (Table 1). The final BDCI of both the YRD and the PRD were determined to be BDC-stratospheric for the same reason. BDCI has

a comparable influence on regional TCO in BTH and the YRD, which is greater than that in the PRD. However, the response of PRD to BDCW ( $\rho = 0.66$ ) is on the stronger side in terms of interregional comparisons.

Although the CCM has detected the causal effect of BDC on the regional TCO, it cannot identify whether the drive is positive or negative. Therefore, correlation analysis was added. Fig. 4 shows standardized deseasonalized and detrended time series of TCO and BDC indices along with their  $\rho$  and the correlation coefficients ( $r$ ).

TCO in BTH and the YRD have significantly negative linear responses to BDCI (Fig. 4a-b), with correlation coefficients of 0.64 and 0.72, respectively. The correlation coefficient between TCO-PRD and BDCI is the lowest ( $r = 0.37$ , Fig. 4c). Given that CCM has detected that BDCI does have a strong driving effect on TCO-PRD ( $\rho = 0.71$ ), low level of correlation coefficients indicates that the response of TCO-PRD to BDCI may include a considerable portion of the nonlinear response. The response of TCO to BDCW is dominated by nonlinear responses in all regions. The correlation coefficients in Fig. 4d-f are all lower than 0.2 with the significance level lower than 95%. Therefore, it is difficult to infer that regional TCO responses are positive or negative to BDCW in

**Fig. 8.** The same as Fig. 4, but for HC.

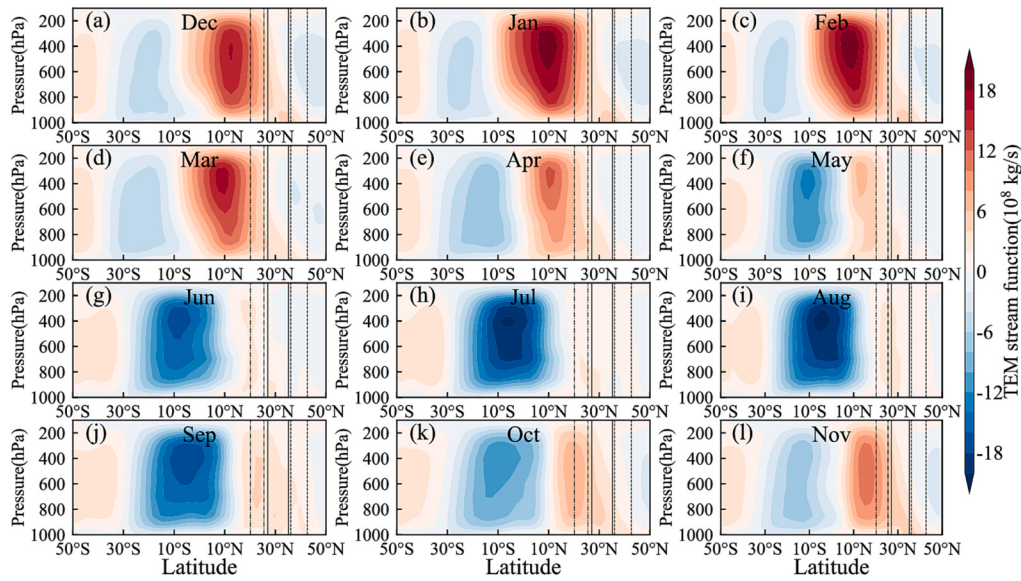


Fig. 9. The same as Fig. 5, but for HC.

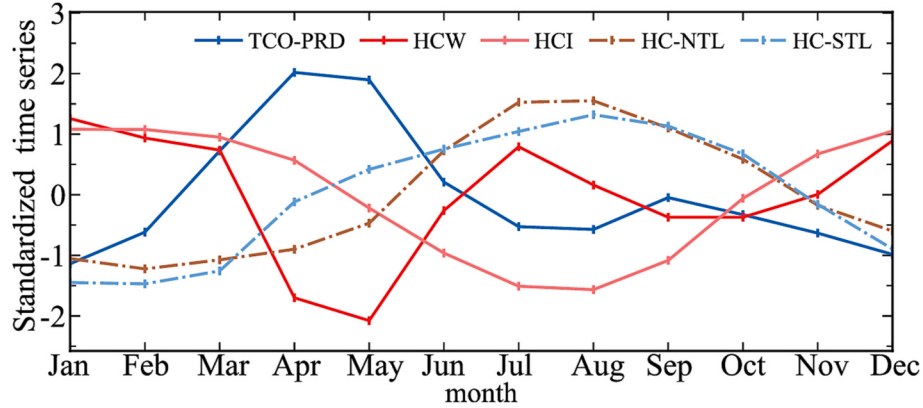


Fig. 10. The same as Fig. 6, but for HC.

these three regions. Overall, the results of the correlation analysis can support the main conclusions of the CCM analysis, including that BDCI has a stronger driving effect on TCO than BDCW, and that the response of TCO-PRD to BDC is significantly weaker than that of the other two regions.

PRD resides chronically inside the BDC upwelling (Fig. 5), which may account for the strong nonlinear response of TCO-PRD to BDCW. The BDCW annual cycle can be further subdivided into two phases with April and September as the boundary. April and September coincide with the two peaks of the TCO-PRD annual cycle (Fig. 2e), making it more convincing that the nonlinear drive of BDC also has unignorable contributions to the temporal variation of TCO-PRD. Fig. 6 shows the annual circulation curve of TCO-PRD along with BDC upwelling width and its north-south boundaries. Both the TCO-PRD and BDCW have significant bimodal structures, with a correlation coefficient reaching  $-0.76$  ( $p < 0.01$ ). Moreover, the occurrence time of the extremes of BDCW and the TCO-PRD coincides nearly perfectly. BDCW and the movement of the upwelling are controlled by the development of BDC in the southern hemisphere from April to September (Fig. 5e-j). During this period, the upwelling center approaches the PRD gradually, with the powerful upward vertical transport contributing to the decline of TCO-PRD (Fig. 6). In general, the BDCW is mainly driven by the boundary of BDC in the winter hemisphere, which furtherly has markedly facilitated the establishment of bimodal structures of the TCO-PRD annual

cycle. In addition, BDCI has a unimodal annual cycle structure consistent with TCO in northerly China, which corresponds to that BDCI drives TCO-BTH and TCO-YRD significantly stronger than BDCW (Fig. 3a-b).

### 3.2.2. The causal influence of HC on TCO in China

Fig. 7 shows the results of TCO mapping HC indices diagnosed by CCM, and their  $\rho$  values are listed in Table 2. All five HC indices exert substantial causal influences on TCO in the study area, with the influence of the HCI greater than that of the HCW. Highly similar to BDC, the causal effect of HC on TCO-PRD is also significantly weaker than that of the other two. However, TCO mapping HCW converges fastest with the most excellent mapping skill among all HC indices, indicating that the TCO-PRD responds more strongly to HCW than HCI. The indistinguishable CCM results of NHC-500 and NHC-250 (Fig. 7) suggest that the causal impact of HC on TCO is insensitive to vertical height, particularly in the middle and upper troposphere. The  $\rho$  value of THC-500 is even lower than that of HCW, suggesting that total HC is notably less influential than hemispherical HC. Using the total HC intensity to examine the impact of HC on TCO in China may result in a great underestimation. Accordingly, NHC-250 was determined as the proxy of HCI in the YRD, and SHC-500 as the final HCI in BTH and the PRD. Taking  $\rho$  values of final proxy indices for comparison, the causal effect of HC on BTH and the YRD was even stronger than that of BDC (Table 1 and Table 2).

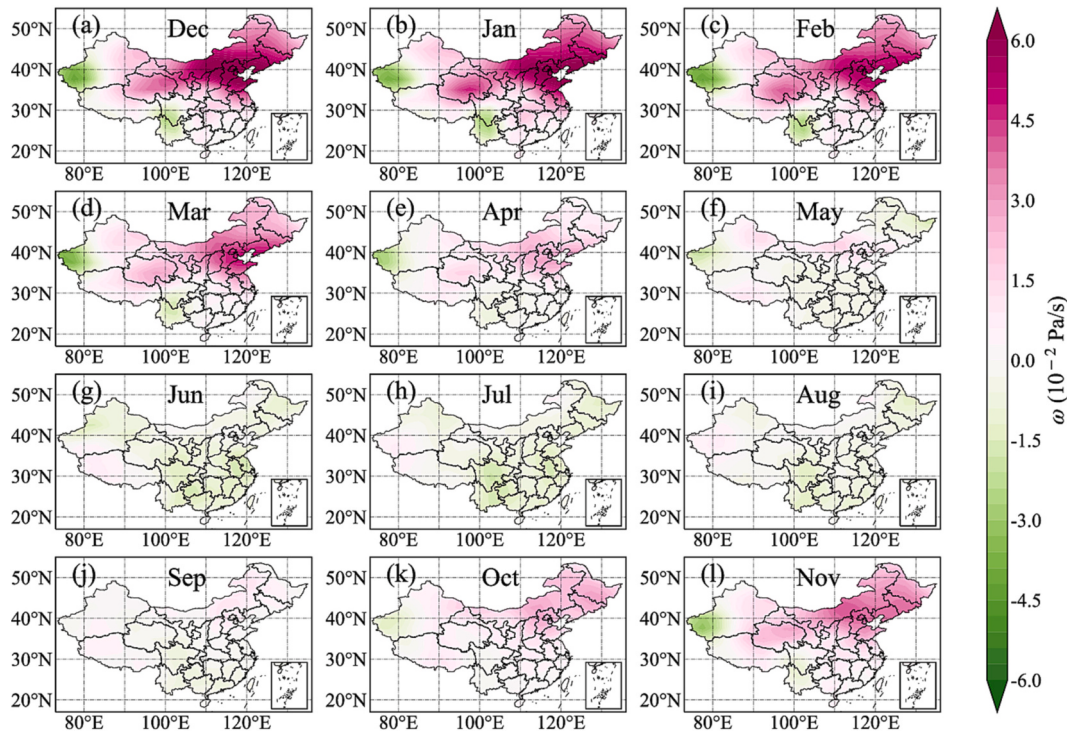


**Fig. 11.** Monthly variation of vertical velocity ( $\omega$ ) at the tropopause over China.

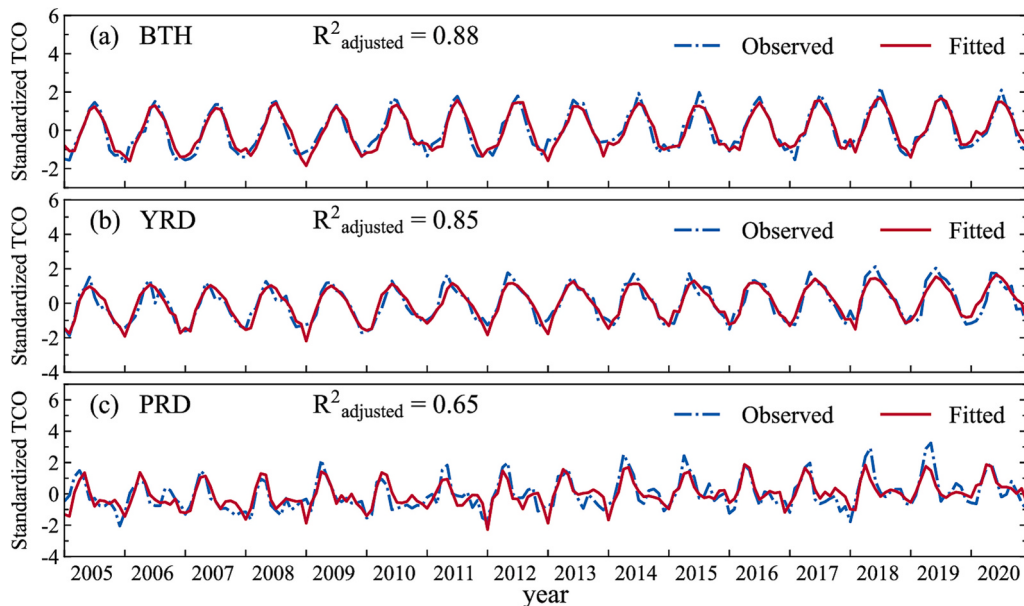


**Fig. 12.** TCO observed by OMI/MLS with the fitted by the MLR model.

The results of the correlation analysis also have many similarities with BDC (Fig. 8), including: (1) TCO-BTH and TCO-YRD response negatively ( $r = -0.7$  and  $-0.63$ , respectively), but not completely linearly, to HCl; (2) The linear correlation between TCO-PRD and HCl ( $r = -0.31$ ) is greatly weaker than that of the other two regions. The difference is that compared to BDCW, HCW exhibits significant negative linear driving components for TCO in all regions, although the correlation coefficients are all relatively lower ( $r = -0.25$ ,  $-0.4$ , and  $-0.37$ , respectively). HCW has an even more strongly negative drive on TCO-PRD than HCl (Fig. 8c and f), which caught our attention again.

Fig. 9 shows the annual cycle of the HC structure. It can also be

divided into two phases, with the cut-off time slightly different from BDC (Fig. 5). However, similar to the BDC upwelling, the upwelling of HC also gradually moves towards the northern hemisphere and crosses PRD from April to September. According to Fig. 10, the negative correlation between TCO-PRD and HCW ( $r^{**} = -0.85$ ) is stronger than that of BDCW ( $r^{**} = -0.76$ ). HC upwelling transports pollutants from the low tropic troposphere to the up layers and into the stratosphere with upward pumping of stratosphere BDC. The vertical velocity at the tropopause is depicted in Fig. 11, confirming that upward transport is strong enough to penetrate the tropopause from May to August in southeast China, which contributes significantly to the summertime decrease in

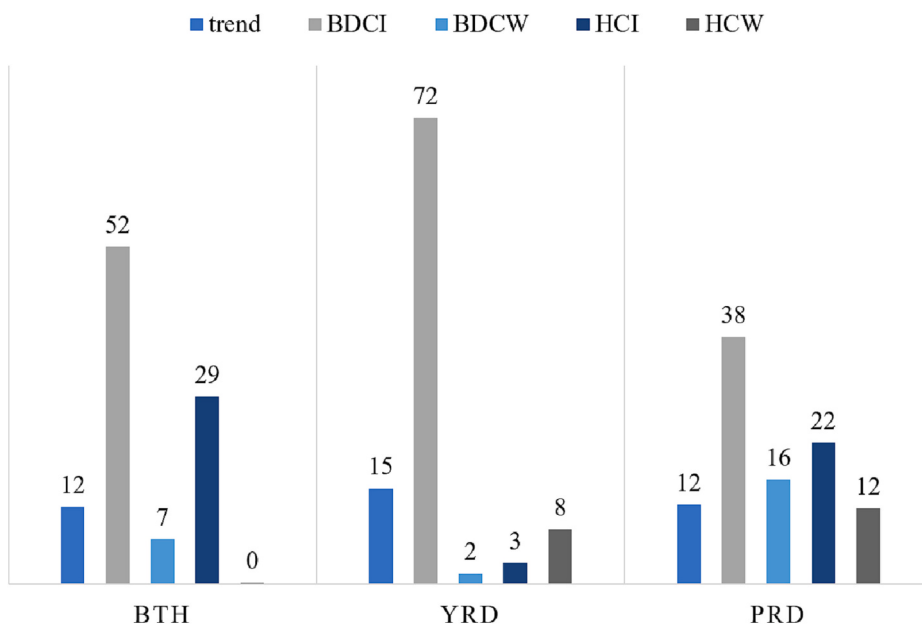


**Fig. 13.** The relative importance (%) of the linear trend, the BDC, and the HC to the regional TCO.

**Table 3**

The standardized regression coefficients of explanatory variables estimated by ridge regression in the MLR model.

	BTH	YRD	PRD
trend	0.137	0.191	0.255
BDCI	-0.601	-0.931	-0.798
BDCW	0.080	0.021	-0.337
HCI	-0.334	0.042	0.456
HCW	0.003	-0.109	-0.244

the TCO-PRD. Thus, in addition to the East Asian summer monsoon (Wang et al., 2021), the meridian circulations including BDC and HC also lead effectively to the formation of the bimodal annual cycle structure of TCO-PRD. They are coupled through mass transport to be a crucial link and channel between the troposphere and stratosphere (Salby and Callaghan, 2005).

### 3.3. The relative contributions of BDC and HC

The CCM analysis confirmed that BDC and HC drive regional TCO significantly in the study area and determined the most appropriate indices that best reflect their causal influence on TCO. On this basis, an MLR model was built to fit OMI/MLS TCO (Fig. 12). The high levels of  $R^2_{\text{adjusted}}$  (0.65–0.88) demonstrate that the selected indices variables can effectively explain the changes in TCO. The relative importance of explanatory variables (Fig. 13) was examined based on standardized regression coefficients (Table 3). Linear trends account for 12–15% of TCO long-term changes from 2005 to 2020 in our study area. However, the BDC and HC played different roles in these regions. In BTH, the circulation intensities derived TCO great stronger than their upwelling width, with relative contributions of 52% and 29%, respectively. In the YRD, TCO long-term change was dominant by BDCI which can explain 72% of the change in regional TCO. For the PRD, the difference in relative contributions of the four meridian circulation indices was relatively smaller, however, the role of BDCI (38%) remains ahead of the others. Differences between the MLR and CCM analysis results may be attributed to the fact that the response of TCO to atmospheric circulation is not entirely linear. The strong linear response of TCO-TRD to BDCI (Fig. 4) may explain its overwhelming importance assessed by the MLR.

Additionally, the MLR model offers a long-term TCO trend during

2005–2020 based on the non-standardized regression coefficients of  $t$  in expression (4). Positive trends of  $2.3 \pm 0.4$ ,  $2.5 \pm 0.3$ , and  $2.7 \pm 0.5$  DU/decade were found in BTH, the YRD, and the PRD, respectively. These Positive trends strongly agree with findings from the Tropospheric Ozone Assessment Report-Climate (Gaudel et al., 2018) and earlier studies (Chen et al., 2020; Ebojje et al., 2016; Ziemke et al., 2019). Modeling studies showed that climate warming would lead to increased tropospheric O<sub>3</sub> levels in overpopulated areas as a result of enhanced biogenic hydrocarbon emissions and accelerated decomposition of peroxyacetyl nitrate (PAN) to form NO<sub>x</sub> at higher temperatures (Doherty et al., 2013; Jacob and Winner, 2009). Our research demonstrated that BDC and HC significantly affect TCO in China, particularly in the PRD. Consequently, the impact of the strengthening and broadening of BDC and HC caused by climate change on the long-term trend in TCO should be valued and further investigated.

### 4. Conclusions

In this study, we analyzed the seasonal variation pattern of TCO in three major city clusters in China based on OMI/MLS data. It is found that the unimodal annual cycle eventually evolves into a bimodal annual cycle as the regional latitude shifts from north to south and the peak season shifts from summer to spring. This study discusses the connection of BDC and HC to TCO in China, which remains poorly understood, based on a novel and powerful causal analysis method. CCM revealed the substantial dynamic coupling of BDC and HC to TCO in China. While TCO responded to hemispherical HC more strongly than THC, there was little difference in the response intensity to different BDC branches. The BDC and HC indices determined by CCM were used for building an MLR model, which quantitatively assessed their importance for long-term changes in regional TCO. BDCI is the most important influencing factor in each region, particularly in the YRD. TCO-BTH is mainly affected by the intensity of the two meridian circulations. The influence of the widths of meridional circulation upwellings on TCO-PRD cannot be ignored. The enormous contribution of BDC and HC to the TCO-PRD benefited from their upward transport, especially in May–August, which promoted the formation of the TCO-PRD bimodal annual cycle pattern. According to the MLR analysis, TCO displayed significant positive trends in our study areas during 2005–2020, with rates of  $2.3 \pm 0.4$ ,  $2.5 \pm 0.3$ , and  $2.7 \pm 0.5$  DU/decade in BTH, the YRD, and the PRD, respectively.

## CRediT authorship contribution statement

**Xin Zhang:** Conceptualization, Methodology, Visualization, Investigation, Formal analysis, Writing – review & editing, Writing – original draft. **Xingying Zhang:** Supervision. **Lihua Zhou:** Writing – review & editing. **Xifeng Cao:** Writing – original draft. **Zhili Deng:** Data curation. **Yuhan Jiang:** Data curation.

## Declaration of Competing Interest

The authors declare that they have no known competing financial interests or personal relationships that could have appeared to influence the work reported in this paper.

## Data availability

Data will be made available on request.

## Acknowledgments

This work is funded by the National Key Research and Development Program Earth Observation and Navigation Key Project (No. 2022YFB3904801) and the National Natural Science Foundation of China (No. 41775028, No. 41805098, and No. 41921005).

## References

- Akossou, A., 2013. Impact of data structure on the estimators R-square and adjusted R-square in linear regression. *Int. J. Mathemat. Computat.* 20, 84–93.
- Andrews, D.G., McIntyre, M.E., 1978. An exact theory of nonlinear waves on a Lagrangian-mean flow. *J. Fluid Mech.* 89, 609–646. <https://doi.org/10.1017/s0022112078002773>.
- Banerjee, A., Archibald, A.T., Maycock, A.C., Telford, P., Abraham, N., Yang, X., Braesicke, P., Pyle, J., 2014. Lightning NO x, a key chemistry–climate interaction: impact of future climate change and consequences for tropospheric oxidising capacity. *Atmos. Chem. Phys.* 14, 9871–9881.
- Bian, J., Yan, R., Chen, H., Lü, D., Massie, S.T., 2011. Formation of the summertime ozone valley over the Tibetan Plateau: the Asian summer monsoon and air column variations. *Adv. Atmos. Sci.* 28, 1318. <https://doi.org/10.1007/s00376-011-0174-9>.
- Butchart, N., 2014. The Brewer-Dobson circulation. *Rev. Geophys.* 52, 157–184.
- Charlesworth, E.J., Birner, T., Albers, J.R., 2019. Ozone transport-radiation feedbacks in the tropical tropopause layer. *Geophys. Res. Lett.* 46, 14195–14202.
- Chen, Z., Zhuang, Y., Xie, X., Chen, D., Cheng, N., Yang, L., Li, R., 2019. Understanding long-term variations of meteorological influences on ground ozone concentrations in Beijing during 2006–2016. *Environ. Pollut.* 245, 29–37. <https://doi.org/10.1016/j.enpol.2018.10.117>.
- Chen, X., Zhong, B., Huang, F., Wang, X., Sarkar, S., Jia, S., Deng, X., Chen, D., Shao, M., 2020. The role of natural factors in constraining long-term tropospheric ozone trends over Southern China. *Atmos. Environ.* 220, 117060 <https://doi.org/10.1016/j.atmosenv.2019.117060>.
- Cooper, O.R., Parrish, D., Ziemke, J., Balashov, N., Cupeiro, M., Galbally, I., Gilge, S., Horowitz, L., Jensen, N., Lamarque, J.-F., 2014. Global Distribution and Trends of Tropospheric Ozone: An Observation-Based reviewGlobal Distribution and Trends of Tropospheric Ozone. *Elemental Science of the Anthropocene*, p. 2.
- Danielsen, Edwin F., 1968. Stratospheric-tropospheric exchange based on radioactivity, ozone and potential vorticity. *J. Atmos. Sci.* 25, 502–518.
- Ding, A., Wang, T., 2006. Influence of stratosphere-to-troposphere exchange on the seasonal cycle of surface ozone at Mount Waliguan in western China. *Geophys. Res. Lett.* 33 <https://doi.org/10.1029/2005GL024760>.
- Doherty, R., Wild, O., Shindell, D., Zeng, G., MacKenzie, I., Collins, W., Fiore, A.M., Stevenson, D., Dentener, F., Schultz, M., 2013. Impacts of climate change on surface ozone and intercontinental ozone pollution: a multi-model study. *J. Geophys. Res. Atmos.* 118, 3744–3763.
- Dufour, G., Eremenko, M., Beekmann, M., Cuesta, J., Foret, G., Fortems-Cheiney, A., Lachatre, M., Lin, W., Liu, Y., Xu, X., Zhang, Y., 2018. Lower tropospheric ozone over the North China Plain: variability and trends revealed by IASI satellite observations for 2008–2016. *Atmos. Chem. Phys.* 18, 16439–16459. <https://doi.org/10.5194/acp-18-16439-2018>.
- Ebojcie, F., Burrows, J.P., Gebhardt, C., Ladstaetter-Weißenmayer, A., von Savigny, C., Rozanov, A., Weber, M., Bovensmann, H., 2016. Global tropospheric ozone variations from 2003 to 2011 as seen by SCIAMACHY. *Atmos. Chem. Phys.* 16, 417–436. <https://doi.org/10.5194/acp-16-417-2016>.
- Fishman, J., Larsen, J.C., 1987. Distribution of total ozone and stratospheric ozone in the tropics: Implications for the distribution of tropospheric ozone. *J. Geophys. Res.-Atmos.* 92, 6627–6634. <https://doi.org/10.1029/JD092D06p06627>.
- Fishman, J., Wozniak, A., Creilson, J., 2003. Global distribution of tropospheric ozone from satellite measurements using the empirically corrected tropospheric ozone residual technique: identification of the regional aspects of air pollution. *Atmos. Chem. Phys.* 3, 893–907.
- Fu, J.S., Dong, X., Gao, Y., Wong, D.C., Lam, Y.F., 2012. Sensitivity and linearity analysis of ozone in East Asia: the effects of domestic emission and intercontinental transport. *J. Air Waste Manage. Assoc.* 62, 1102–1114.
- Fu, Q., Lin, P., Solomon, S., Hartmann, D., 2015. Observational evidence of strengthening of the Brewer-Dobson circulation since 1980. *J. Geophys. Res.-Atmos.* 120, 10214–210228.
- Fu, Y., Liao, H., Yang, Y., 2019. Interannual and decadal changes in tropospheric ozone in China and the associated chemistry-climate interactions: a review. *Adv. Atmos. Sci.* 36, 975–993. <https://doi.org/10.1007/s00376-019-8216-9>.
- Gao, M., Gao, J., Zhu, B., Kumar, R., Lu, X., Song, S., Zhang, Y., Jia, B., Wang, P., Beig, G., Hu, J., Ying, Q., Zhang, H., Sherman, P., McElroy, M.B., 2020. Ozone pollution over China and India: seasonality and sources. *Atmos. Chem. Phys.* 20, 4399–4414. <https://doi.org/10.5194/acp-20-4399-2020>.
- Gaudel, A., Cooper, O.R., Ancellet, G., Barret, B., Boynard, A., Burrows, J.P., Clerbaux, C., Coheur, P.-F., Cuesta, J., Cuevas, E., Doniki, S., Dufour, G., Ebojcie, F., Foret, G., Garcia, O., Granados-Muñoz, M.J., Hannigan, J.W., Hase, F., Hassler, B., Huang, G., Hurtmans, D., Jaffe, D., Jones, N., Kalabokas, P., Kerridge, B., Kulawik, S., Latter, B., Leblanc, T., Le Flochmoën, E., Lin, W., Liu, J., Liu, X., Mahieu, E., McClure-Begley, A., Neu, J.L., Osman, M., Palm, M., Petetin, H., Petropavlovskikh, I., Querel, R., Rahpoe, N., Rozanov, A., Schultz, M.G., Schwab, J., Siddans, R., Smale, D., Steinbacher, M., Tanimoto, H., Tarasick, D.W., Thouret, V., Thompson, A.M., Triclk, T., Weatherhead, E., Wespes, C., Worden, H.M., Vigouroux, C., Xu, X., Zeng, G., Ziemke, J., 2018. Tropospheric ozone assessment report: present-day distribution and trends of tropospheric ozone relevant to climate and global atmospheric chemistry model evaluation. *Elementa: Sci. Anthropocene.* 6 <https://doi.org/10.1525/elementa.291>.
- Granger, C.W.J., 1969. Investigating causal relations by econometric models and cross-spectral methods. *Econometrica: J. Econometr. Soc.* 424–438.
- Grunke, N.E., Heath, R.L., 2020. Ozone effects on plants in natural ecosystems. *Plant Biol.* 22, 12–37. <https://doi.org/10.1111/plb.12971>.
- Hilt, D.E., Seegrist, D.W., 1977. Ridge, a Computer Program for Calculating Ridge Regression Estimates. Department of Agriculture, Forest Service, Northeastern Forest Experiment ....
- Holton, J.R., 1990. On the Global Exchange of Mass between the Stratosphere and Troposphere Journal of Atmospheric Sciences, 47, pp. 392–395. [https://doi.org/10.1175/1520-0469\(1990\)047<0392:Otgeom>2.0.Co;2](https://doi.org/10.1175/1520-0469(1990)047<0392:Otgeom>2.0.Co;2).
- Holton, J.R., Haynes, P.H., McIntyre, M.E., Douglass, A.R., Rood, R.B., Pfister, L., 1995. Stratosphere-troposphere exchange. *Rev. Geophys.* 33, 403–439. <https://doi.org/10.1029/95RG02097>.
- Hsu, J., Prather, M.J., 2009. Stratospheric variability and tropospheric ozone. *J. Geophys. Res.-Atmos.* 114 <https://doi.org/10.1029/2008JD010942>.
- Hsu, J., Prather, M.J., Wild, O., 2005. Diagnosing the stratosphere-to-troposphere flux of ozone in a chemistry transport model. *J. Geophys. Res.-Atmos.* 110.
- Hu, Y., Fu, Q., 2007. Observed poleward expansion of the Hadley circulation since 1979. *Atmos. Chem. Phys.* 7, 5229–5236.
- Hu, Y., Tao, L., Liu, J., 2013. Poleward expansion of the Hadley circulation in CMIP5 simulations. *Adv. Atmos. Sci.* 30, 790–795.
- Hu, Y., Yan, H., Zhang, X., Gao, Y., Zheng, X., Liu, X., 2020. Study on calculation and validation of tropospheric ozone by ozone monitoring instrument – microwave limb sounder over China. *Int. J. Remote Sens.* 41, 9101–9120. <https://doi.org/10.1080/01431161.2020.1800012>.
- Huajun, L., Guangjie, D., 2018. Research on spatial correlation of haze pollution in China. *Stat. Res.* 35, 3.
- Huang, J., Zhou, C., Lee, X., Bao, Y., Zhao, X., Fung, J., Richter, A., Liu, X., Zheng, Y., 2013. The effects of rapid urbanization on the levels in tropospheric nitrogen dioxide and ozone over East China. *Atmos. Environ.* 77, 558–567. <https://doi.org/10.1016/j.atmosenv.2013.05.030>.
- IPCC, 2021. Climate change 2021 - the physical science basis. *Interaction.* 49, 44–45.
- Jacob, D.J., Winner, D.A., 2009. Effect of climate change on air quality. *Atmos. Environ.* 43, 51–63.
- Lelieveld, J., Dentener, F.J., 2000. What controls tropospheric ozone? *J. Geophys. Res.-Atmos.* 105, 3531–3551.
- Li, R., Xu, M., Li, M., Chen, Z., Zhao, N., Gao, B., Yao, Q., 2021. Identifying the spatiotemporal variations in ozone formation regimes across China from 2005 to 2019 based on polynomial simulation and causality analysis. *Atmos. Chem. Phys.* 21, 15631–15646. <https://doi.org/10.5194/acp-21-15631-2021>.
- Liao, Z., Ling, Z., Gao, M., Sun, J., Zhao, W., Ma, P., Quan, J., Fan, S., 2021. Tropospheric ozone variability over Hong Kong based on recent 20 years (2000–2019) ozonesonde observation. *J. Geophys. Res.-Atmos.* 126 <https://doi.org/10.1029/2020JD033054>.
- Lin, P., Fu, Q., 2013. Changes in various branches of the Brewer-Dobson circulation from an ensemble of chemistry climate models. *J. Geophys. Res.-Atmos.* 118, 73–84.
- Liu, Y., Zhang, Y., Wang, Y., Liu, C., Cai, Z., Konopka, P., Müller, R., 2015. Dominant modes of tropospheric ozone variation over East Asia from GOME observations. *Adv. Meteorol.* 2015.
- Liu, N., Lin, W., Ma, J., Xu, W., Xu, X., 2019. Seasonal variation in surface ozone and its regional characteristics at global atmosphere watch stations in China. *J. Environ. Sci.* 77, 291–302. <https://doi.org/10.1016/j.jes.2018.08.009>.
- Lu, X., Zhang, L., Chen, Y., Zhou, M., Zheng, B., Li, K., Liu, Y., Lin, J., Fu, T.-M., Zhang, Q., 2019a. Exploring 2016–2017 surface ozone pollution over China: source contributions and meteorological influences. *Atmos. Chem. Phys.* 19, 8339–8361.
- Lu, X., Zhang, L., Zhao, Y., Jacob, D.J., Hu, Y., Hu, L., Gao, M., Liu, X., Petropavlovskikh, I., McClure-Begley, A., 2019b. Surface and tropospheric ozone

- trends in the Southern Hemisphere since 1990: possible linkages to poleward expansion of the Hadley circulation. *Sci. Bull.* 64, 400–409.
- Ma, J., Zheng, X., Xu, X., 2005. Comment on “why does surface ozone peak in summertime at Waliguan?” by Bin Zhu et al. *Geophys. Res. Lett.* 32, L01805.
- MEEPRC, 2022. Report on the State of the Ecology and Environment in China. Ministry of Ecology and Environment of the People’s Republic of China. <https://www.mee.gov.cn/hjzl/sthjzk/zghjzkgb/>.
- Nuvolone, D., Petri, D., Voller, F., 2018. The effects of ozone on human health. *Environ. Sci. Pollut. Res.* 25, 8074–8088.
- Okamoto, S., Tanimoto, H., 2016. A review of atmospheric chemistry observations at mountain sites. *Progr. Earth Planet. Sci.* 3, 34. <https://doi.org/10.1186/s40645-016-0109-2>.
- Pikovnik, M., Zaplotnik, Ž., Boljka, L., Žagar, N., 2022. Metrics of the Hadley circulation strength and associated circulation trends. *Weather Clim. Dynam. 3*, 625–644. <https://doi.org/10.5194/wcd-3-625-2022>.
- Rosenlof, K.H., 1995. Seasonal cycle of the residual mean meridional circulation in the stratosphere. *J. Geophys. Res.-Atmos.* 100, 5173–5191. <https://doi.org/10.1029/94JD03122>.
- Salby, M.L., Callaghan, P.F., 2005. Interaction between the Brewer-Dobson circulation and the Hadley circulation. *J. Clim.* 18, 4303–4316. <https://doi.org/10.1175/JCLI3509.1>.
- Shu, L., Wang, T., Han, H., Xie, M., Chen, P., Li, M., Wu, H., 2020. Summertime ozone pollution in the Yangtze River Delta of eastern China during 2013–2017: synoptic impacts and source apportionment. *Environ. Pollut.* 257, 113631 <https://doi.org/10.1016/j.envpol.2019.113631>.
- Stevenson, D., Young, P., Naik, V., Lamarque, J.-F., Shindell, D.T., Voulgarakis, A., Skeie, R.B., Dalsoren, S.B., Myhre, G., Berntsen, T.K., 2013. Tropospheric ozone changes, radiative forcing and attribution to emissions in the Atmospheric Chemistry and climate Model Intercomparison Project (ACCMIP). *Atmos. Chem. Phys.* 13, 3063–3085.
- Stohl, A., Bonasoni, P., Cristofanelli, P., Collins, W., Feichter, J., Frank, A., Forster, C., Gerasopoulos, E., Gäggeler, H., James, P., Kentarchos, T., Kromp-Kolb, H., Krüger, B., Land, C., Meloen, J., Papayannnis, A., Priller, A., Seibert, P., Sprenger, M., Roelofs, G.J., Scheel, H.E., Schnabel, C., Siegmund, P., Tobler, L., Triclk, T., Wernli, H., Wirth, V., Zanis, P., Zerefos, C., 2003. Stratosphere-troposphere exchange: a review, and what we have learned from STACCATO. *J. Geophys. Res.-Atmos.* 108 <https://doi.org/10.1029/2002JD002490>.
- Sugihara, G., May, R., Ye, H., Hsieh, C.H., Deyle, E., Fogarty, M., Munch, S., 2012. Detecting causality in complex ecosystems. *Science* 338, 496–500. <https://doi.org/10.1126/science.1227079>.
- Takens, F., 2006. Detecting strange attractors in turbulence. In: *Dynamical Systems and Turbulence, Warwick 1980: Proceedings of a symposium held at the University of Warwick 1979/80*. Springer, pp. 366–381.
- Tang, G., Wang, Y., Li, X., Ji, D., Hsu, S., Gao, X.J.A.C., 2012. Spatial-temporal variations in surface ozone in Northern China as observed during 2009–2010 and possible implications for future air quality control strategies. *Atmos. Chem. Phys.* 12, 2757–2776.
- Wang, Y., Hu, B., Tang, G., Ji, D., Zhang, H., Bai, J., Wang, X., Wang, Y., 2013. Characteristics of ozone and its precursors in Northern China: a comparative study of three sites. *Atmos. Res.* 132, 450–459.
- Wang, H., Wang, W., Huang, X., Ding, A., 2020. Impacts of stratosphere-to-troposphere-transport on summertime surface ozone over eastern China. *Sci. Bull.* 65, 276–279.
- Wang, Y., Shen, J., Wang, H., Wu, G., Chen, Y., Liu, T., Gong, D., Ou, J., Shi, Y., Zhang, T., He, C., Chen, D., Wang, B., 2021. Unexpected seasonal variations and high levels of ozone observed at the summit of Nanling Mountains: impact of Asian monsoon on southern China. *Atmos. Environ.* 253, 118378 <https://doi.org/10.1016/j.atmosenv.2021.118378>.
- Webster, P.J., 2004. The elementary Hadley circulation. In: *The Hadley circulation: Present, Past and Future*. Springer, pp. 9–60.
- Weiguo, W., Fangyuan, Y., Haoyue, W., Tao, Y., Ke, Y., Shukun, L., Wenxuan, F., 2015. The distribution characters of the stratospheric Brewer-Dobson circulation inferred from era-interim. *Chin. J. Geophys.* 58, 20–31.
- Wespes, C., Hurtmans, D., Emmons, L.K., Safieddine, S., Clerbaux, C., Edwards, D.P., Coheur, P.-F., 2016. Ozone variability in the troposphere and the stratosphere from the first 6 years of IASI observations (2008–2013). *Atmos. Chem. Phys.* 16, 5721–5743.
- Yan, F., Gao, Y., Ma, M., Liu, C., Ji, X., Zhao, F., Yao, X., Gao, H., 2021. Revealing the modulation of boundary conditions and governing processes on ozone formation over northern China in June 2017. *Environ. Pollut.* 272, 115999 <https://doi.org/10.1016/j.envpol.2020.115999>.
- Zhang, W., Zou, Y., Zheng, X.D., Wang, N., Yan, H., Chen, Y.P., Zhao, X.J., Ji, Z.P., Li, F., Mai, B.R., Yin, C.Q., Deng, T., Fan, L.Y., Deng, X.J., 2021. Characteristics of the vertical distribution of tropospheric ozone in late autumn at Yangjiang station in Pearl River Delta (PRD), China. PartI: observed event. *Atmos. Environ.* 244, 117898 <https://doi.org/10.1016/j.atmosenv.2020.117898>.
- Zhao, C., Wang, Y., Yang, Q., Fu, R., Cunnold, D., Choi, Y., 2010. Impact of East Asian summer monsoon on the air quality over China: view from space. *J. Geophys. Res.-Atmos.* 115 <https://doi.org/10.1029/2009JD012745>.
- Zhao, K., Hu, C., Yuan, Z., Xu, D., Zhang, S., Luo, H., Wang, J., Jiang, R., 2021. A modeling study of the impact of stratospheric intrusion on ozone enhancement in the lower troposphere over the Hong Kong regions, China. *Atmos. Res.* 247, 105158 <https://doi.org/10.1016/j.atmosres.2020.105158>.
- Zhou, L., Zhang, J., Zheng, X., Xue, W., Zhu, S., 2019. Impacts of chemical and synoptic processes on summer tropospheric ozone trend in North China. *Adv. Meteorol.* 2019, 1–14. <https://doi.org/10.1155/2019/3148432>.
- Ziemke, J.R., Chandra, S., Bhartia, P.K., 1998. Two new methods for deriving tropospheric column ozone from TOMS measurements: assimilated UARS MLS/ HALOE and convective-cloud differential techniques. *J. Geophys. Res.-Atmos.* 103, 22115–22127. <https://doi.org/10.1029/98jd01567>.
- Ziemke, J.R., Chandra, S., Duncan, B.N., Froidevaux, L., Bhartia, P.K., Levelt, P.F., Waters, J.W., 2006. Tropospheric ozone determined from aura OMI and MLS: evaluation of measurements and comparison with the global modeling initiative’s chemical transport model. *J. Geophys. Res.-Atmos.* 111, D19303. <https://doi.org/10.1029/2006jd007089>.
- Ziemke, J.R., Oman, L.D., Strode, S.A., Douglass, A.R., Olsen, M.A., McPeters, R.D., Bhartia, P.K., Froidevaux, L., Labow, G.J., Witte, J.C., 2019. Trends in global tropospheric ozone inferred from a composite record of TOMS/OMI/MLS/OMPS satellite measurements and the MERRA-2 GMI simulation. *Atmos. Chem. Phys.* 19, 3257–3269.